Acta Geophysica (2024) 72:807–827
https://doi.org/10.1007/s11600-023-01133-1

RESEARCH ARTICLE - APPLIED GEOPHYSICS

Surface and subsurface structural mapping for delineating the active emergency spillway fault, Aswan, Egypt, using integrated geophysical data

Mohamed El Bohoty[1] · Essam Ghamry[1] · Ahmed Hamed[1,2] · Mohamed Khalifa[1] · Ayman Taha[1] · Ahmed Meneisy[3,4]

Received: 7 December 2022 / Accepted: 26 May 2023 / Published online: 19 July 2023

Abstract
The High Dam is one of the world's biggest embankments dams. Moreover, the new city of Aswan, which locates on the western side of the Nile River, is one of the cities that was established to overcome the growing population problem. Therefore, the detailed geophysical studies for the active faults are of more importance for assessing the seismic stability for both of them. Indeed, the emergency spillway fault was documented as a normal and inactive fault. While, a moderate earthquake ($M_L = 4.6$) was recorded along this fault in 2010, about 4.5 km away from the Dam. Hence, its activity must be re-evaluated. The seismic activity along the fault and its extension has been studied. The seismicity distributions and the fault plane solution indicate normal faulting with a strike-slip component and shallow focal depth. Moreover, pore pressure and fluid diffusion play an essential role in fault activation process. On the other hand, the magnetic data for the research area was subjected to a detailed analysis. 2D spectrum analysis and 3D Euler deconvolution methods, were used to analyze and interpret the aeromagnetic anomaly data so as to better understand the tectonic framework of the study region. Finally, the integrated geophysical data delineate the trend of the emergency spillway fault which extends NW–SE. This fault could assist in updating the current seismic source model around the High Dam and new Aswan city for evaluating the seismic hazard for both of them.

Keywords High Dam · Seismic stability · Emergency spillway fault · Pore pressure · Aeromagnetic anomaly · 3D Euler deconvolution

Introduction

The assessment of seismic stability and geotechnical characteristics is of utmost importance for the construction of large-scale projects such as dam constructions, nuclear plants, in addition to archeological inspection and preservation and establishment of new cities (Fat-Helbary et al. 2019a, b; Hamed 2019; Abbas et al. 2023). Many geophysical methods are used to determine the buried faults (ex. magnetic, electric, seismic and gravity etc.) one of these methods could be mentioned here is the gravity method in which the steerable filters that are applied to gravity anomaly data, it is effective, rapid, and affordable tool used by geoscientists to identify and locate hidden faults. A significant density disparity for geological structure is seen where there is a hidden fault (Görgün and Albora 2017). Seismology, magnetic and electro-magnetic methods also used for this purpose. In this regard, extensive geophysical and seismic investigations have been conducted to delineate the active faults surrounding the High Dam and the populated cities, including New Aswan city (Fig. 1). Numerous studies have been carried out to determine the traces and seismic activity of these faults, with magnetic methods playing a significant role in identifying their depths and extensions, particularly

Edited by Prof. Bogdan Mihai Niculescu (ASSOCIATE EDITOR) / Prof. Gabriela Fernández Viejo (CO-EDITOR-IN-CHIEF).

✉ Mohamed Khalifa
mohamed.khalifa@nriag.sci.eg

[1] National Research Institute of Astronomy and Geophysics, Helwan, Egypt

[2] Aswan Regional Earthquake Research Center, Aswân, Egypt

[3] Department of Geology, Faculty of Science, Aswan University, Aswân, Egypt

[4] Department of Earth Resources Engineering, Faculty of Engineering, Kyushu University, Fukuoka, Japan

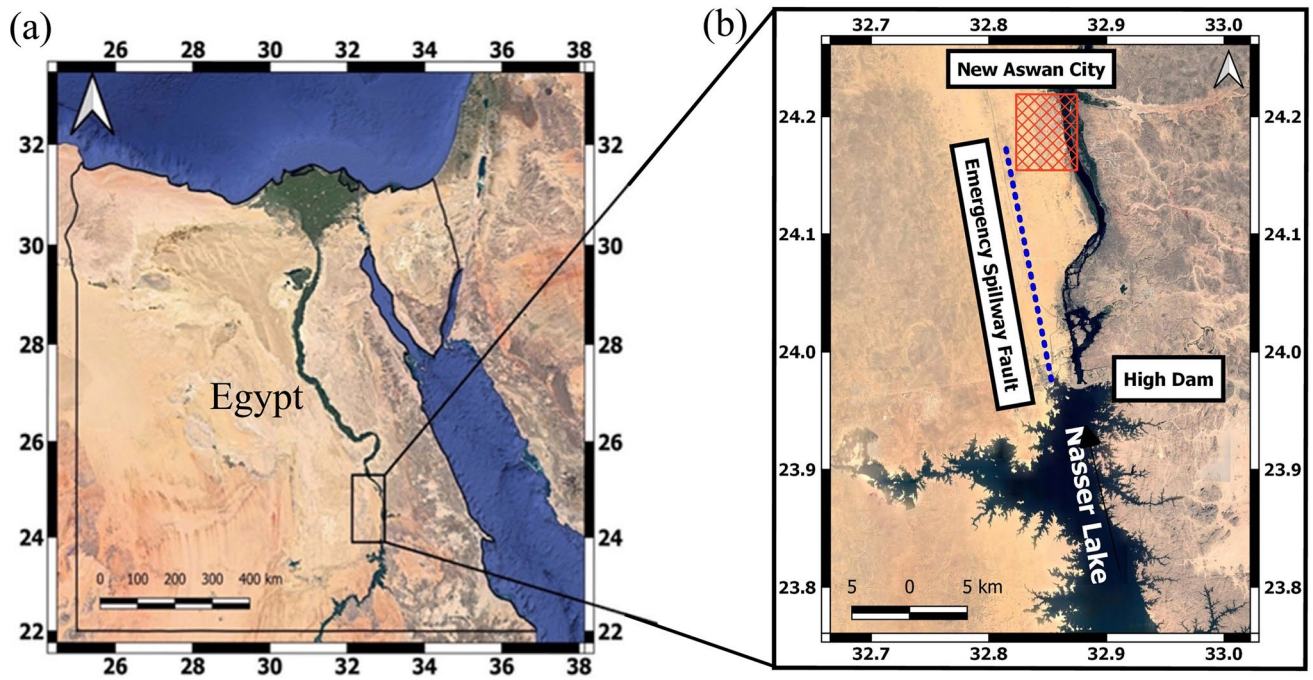

Fig. 1 Location map of the study area

through modern technologies and advanced software. The purpose of applying magnetic methods in this research is to study the subsurface structures around the High Dam, and the new Aswan city.

Based on satellite imaging and ground penetrating radar measurements (GPR) Gaber et al. (2011) determined two sets of faults (NW–SE and E–W) according to the remarkable displacement in the subsurface strata. These faults are said to be related to the Nile River via Wadi El- Kubbaniya, and might potentially constitute ideal groundwater accumulation zones. Saleh (2011) used quantitative and qualitative analysis techniques to estimate the location and depth of the buried source north of Nasser Lake region using Bouguer and seismicity data. He noticed the shallow depth estimation to the top of the basement complex and/or intrusions ranges between 0.3 and 0.8 km, and that the area is influenced by faults trending NW–SE, E–W, N–S, and NE–SW. Furthermore, the area is dissected by a set of basement uplifts and troughs, which are primarily controlled by the NW–SE faults. Koch et al. (2012) corroborated these outcomes and deduced a series of notable structures that mostly lie in the NW–SE and N–S directions and they are generally shorter and less pronounced. In addition, satellite radar data, along with field-based radar analysis, indicated a significant concentration of fracture groups, mostly running in a NW–SE direction. Abdelazeem et al. (2014) investigated the hazardous subsurface structures that control the south Aswan area and their causative source depths using normalized standard deviation filters and deconvolution techniques. They investigated that the area began a hazardous cycle of activity ($M_L > 4$) that could continue over the next few years. On the other hand, the Transient Electromagnetic Method (TEM) soundings used by Geoshy (2020) have been displayed in 2D cross-sections. He deduced from the corresponding vertical discontinuity of the strata of the shale layers of the Dakhla Formation, eight normal faults striking the Gallaba plain (north–west of New Aswan city).

The current research will use the magnetic and earthquake data to delineate the trace of the emergency spillway fault, in order to assess its geo-hazardous effect on the High Dam and New Aswan city. For achieving this goal, the relation between the estimated structural elements deduced from the potential field data with the analysis of the epicentral map of the area and the new updated seismic catalogue of the Aswan seismic network together with the water level fluctuations (1981–2021) that affect the area will be discussed and correlated.

Geology and tectonic setting

The majority of the surface trace of the fault is hidden by sand dune, according to the emergency spillway area map (HADA Report 169 1966). The sediments, on the other hand, cover the fault path locally (Fig. 2). The cross-section that crosses the emergency spillway fault has an easterly-facing topographical scarp (WCC 1985). The scarp is about 10 m high and is displaced to the east. According to a report

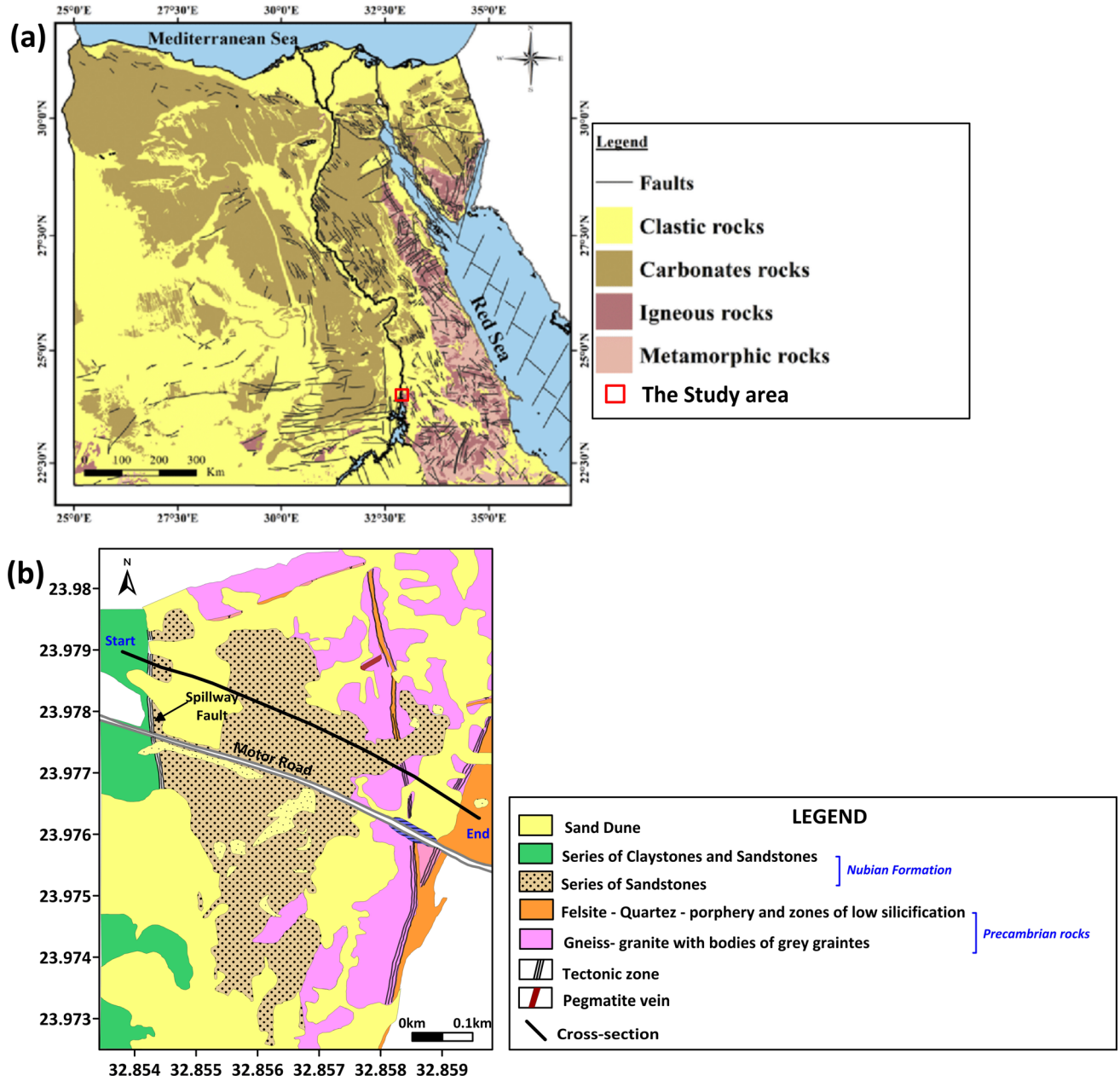

Fig. 2 The geological maps: **a** all Egypt, **b** the emergency spillway fault study area

issued by HADA and Soviet geologists for an assessment of the spillway region (HADA Report 169 1966), the Nubia Formation beds dips about 20° in an area almost 50 m width on the western side of the fault. In other sites around the dam, the bedding in the Nubia Formation is almost horizontal. On a dip-slip fault, inclined strata however, are compatible with drag folding. Displacement on the emergency spillway fault probably occurred prior to the erosion of the Nubia Plan, estimated to be pre-Pliocene in age based on the presence of Pliocene deposits in the area. The vertical cross-section through the emergency spillway fault demonstrates that the fault is vertical (Fig. 3), but probably dips steeply to the west. Furthermore, the western portion of the emergency spillway fault zone showed subsidence, while the eastern part shows uplift (WCC 1985).

Because it is located in the African Platform with its Precambrian folded base, the present research area is structurally associated to the African Orogenic belt

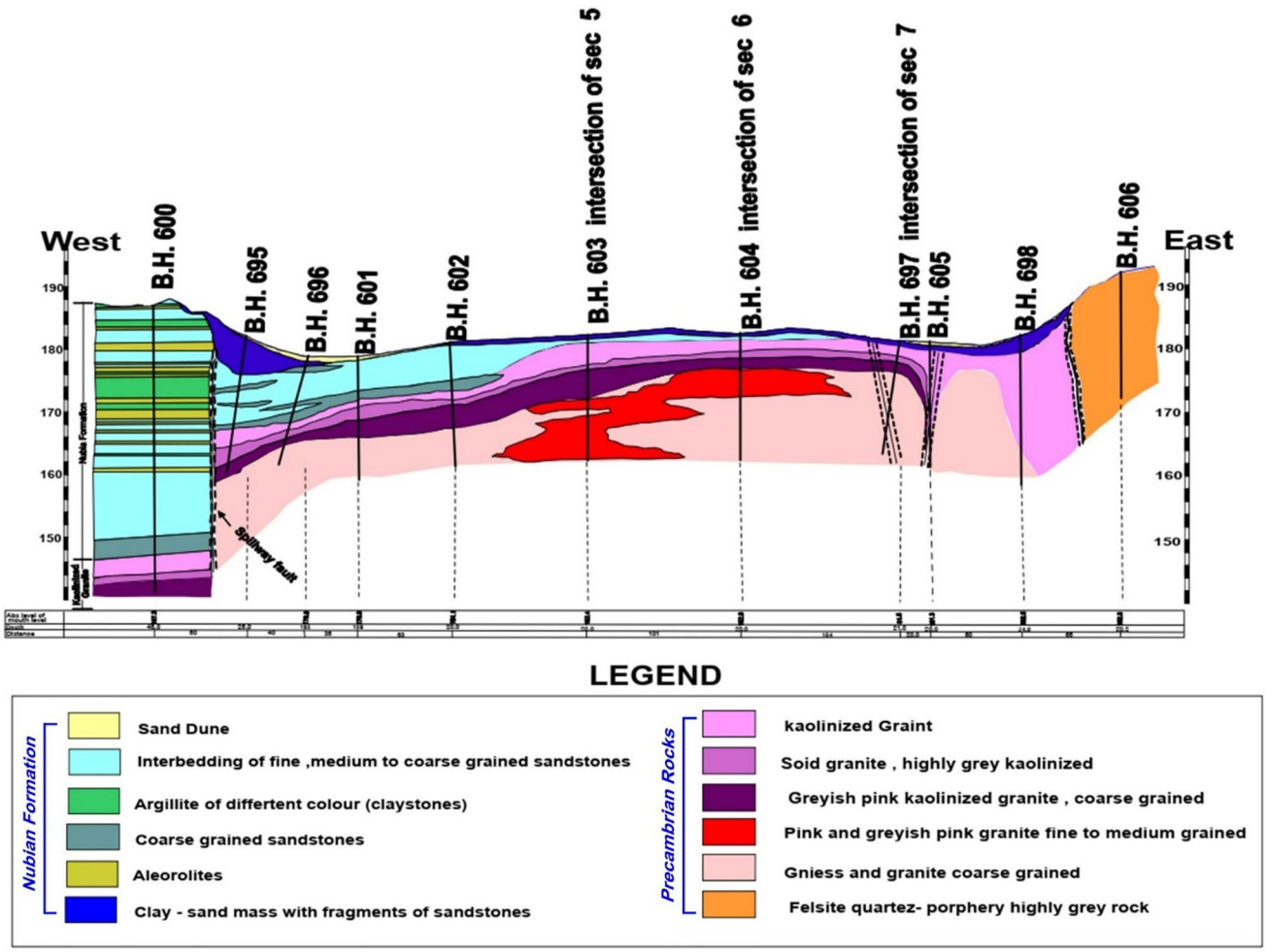

Fig. 3 Cross-section along the spillway fault (WCC 1985)

(Said 1962). The study region is a segment of Egypt's Nile Valley where torque faults parallel to the Aqaba and Suez Gulfs (Youssef 1968). The faults are located North of Nasser lake (ex. Kalabsha, Seiyal, Kurkur, and Khor el-Ramla faults) have all been identified as important to the Aswan High Dam (Kebeasy et al. 1987) (Fig. 4a, b). While the emergency spillway fault is not significant to the seismic hazard assessment for the High Dam according to WCC (1985), while the current seismic activity demonstrates the reverse. The analysis of remote sensing images revealed the probability of the well-known surface trace of the emergency spillway fault zone extended to the west of New Aswan city, and continue to the north-west (Fig. 5). From the satellite image, the fault trace measures about 92 km in length. In the current study it represents a fault zone that strikes towards the NW–SE direction where its trace starts from the western side of the High Dam. The structural type of the Nubian Fault system in the north-west of Aswan, as well as the focal mechanism for moderate to minor earthquakes have been revealed using realistic geology maps and subsurface seismic assessment (Dahy et al. 2009; Fat-Helbary and Haggag 2004; Dahy 2012; Sakran et al. 2018).

Materials and methods

Seismicity data

Seismicity background for Nasser lake

Egypt is a low to moderate seismicity region, so far it has been hit by a few severe earthquakes. Ambraseys et al. (1994) inspect the area covers 300 km around the Aswan High Dam, and he found no historical earthquakes until 1900, while Maamoun et al. (1984) discovered pair of

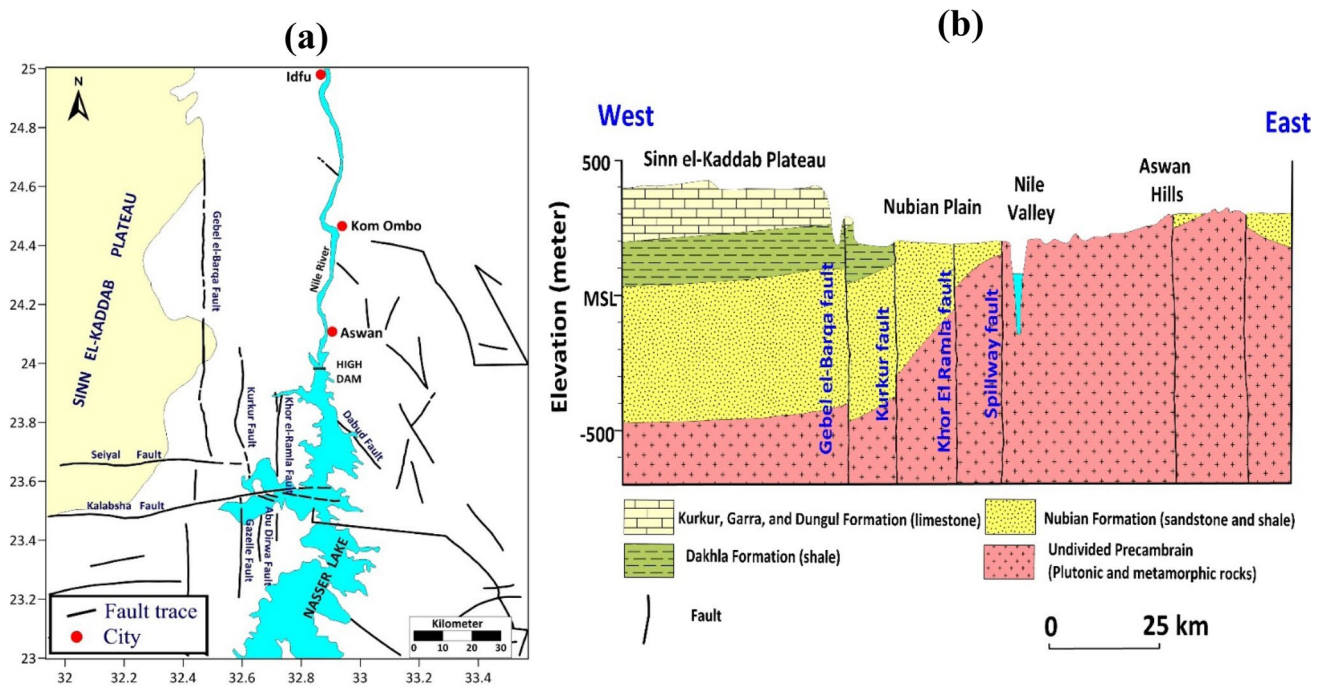

Fig. 4 Structural map of the study area, modified after Egyptian Geological Survey and Mining Authority (EGSMA) (1981) and Woodward-Clyde Consultant (WCC) (1985) (**a**), cross-section along latitude 24° Woodward-Clyde Consultant (WCC) (1985) (**b**)

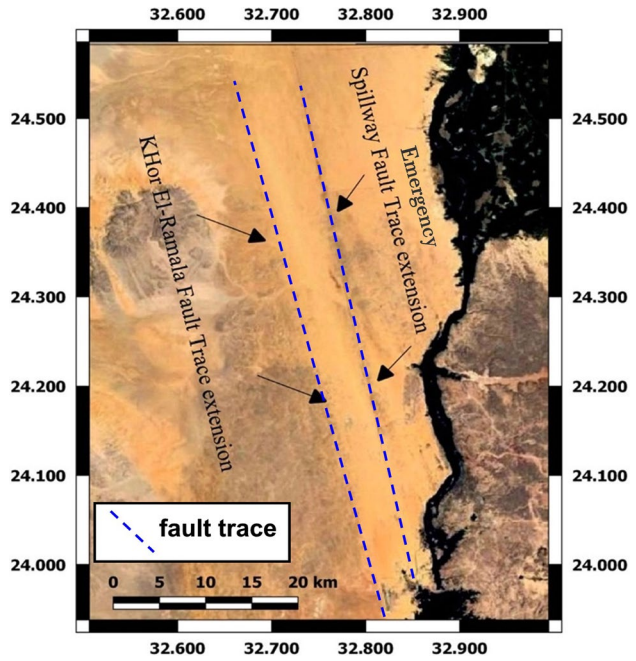

Fig. 5 Landsat-8 image for the emergency spillway fault area

earthquakes of epicentral intensity VII near the epicentre of the 1981 earthquake. In 1210 BC and 1854 AD, two earthquakes struck the same area (Maamoun et al. 1984). A significant earthquake ($M_L = 5.4$) struck recently the northern part of Nasser Lake in 1981, which located along the Kalabsha fault, about 60 km southwest of the High Dam (Kebeasy 1987). Consequently, a scientific bilateral cooperation has been established between the National Research Institute of Astronomy and Geophysics and the authority of the High and Old Aswan Dams to install a seismic network in the Aswan area around the epicentre of the earthquake (Fig. 6), for monitoring the seismic activity north of Nasser Lake since 1981 till today (Fig. 7). Long-term seismological investigations revealed that Nasser Lake has influenced the Aswan region's tectonic stability (Kebeasy 1987; Marlina et al. 2003). As a consequence of the geo-hazardous influence of seismic activity on the Aswan area's infrastructure, the tectonics features (faults) that govern the southern part of Aswan have received considerable attention since 1981. Potential field data such as gravity, magnetic, and electrical studies were frequently used to illustrate the relation between the faulting system and seismicity (e.g., Jeffrey 2011; Mekkawi et al. 2008; Merlina et al. 2003). One of these faults is the emergency spillway fault (WCC 1985), which runs about NW–SE and is one kilometre west of the emergency spillway barrage of the High Dam (Fig. 5).

Seismicity dataset and analysis

The emergency spillway fault is described as a normal and fault with a length of 4 km by HADA and Soviet geologists, and it is documented as an inactive fault that is not

important to the seismic hazard assessment for the High Dam. Dramatically, on November 7, 2010, a magnitude 4.6 earthquake occurred along the emergency spillway fault. It was felt across the Aswan city, and it was accompanied by a huge sound like explosion (Badreldin et al. 2019; Dahy 2012; Primary Report 2010). Therefore, its activity must be re-evaluated for the safety and seismic stability of the High Dam and other cities. The main earthquake and its aftershocks were observed using the Aswan local seismic network (Fig. 6). Consequently, the current field inspection and the previous studies have been done by Soviet scientists for tracing the surface and subsurface structures in and around the Kalabsha seismic active area (Dahy 2012). Moreover, from the relocation of the main earthquake and its aftershocks, we found that the main earthquake is located about 4.5 km northwest of the High Dam, along the emergency spillway fault between the High and Old Aswan Dams. The original source parameter of the selected earthquakes from 1981 to 2021 is relocated accurately using HYPOINVERSE program (Klein 1978), a location program written and used by the United States Geological Survey (USGS), to locate earthquakes and calculate magnitudes. Also, the Root Mean Square Error (RMSE), the horizontal error (ERH), and the vertical error (ERZ) have been quantified and estimated to be as less as possible. On the other hand, the density ρ, the P-wave velocity Vp, and the S-wave velocity Vs used here are taken from Khalil et al. (2004) velocity structure model for Aswan region.

The present study shows that the earthquakes along the emergency spillway fault are roughly concentrated at the NW–SE direction (Fig. 8). According to the obtained cross-sections along the emergency spillway fault over the whole time period (1982–2021), we noticed that the seismicity is characterized by shallow depth, with an average focal depth of 7 km (Fig. 9). A notable decrease in magnitude and an increase in the number of seismic events can be seen in the

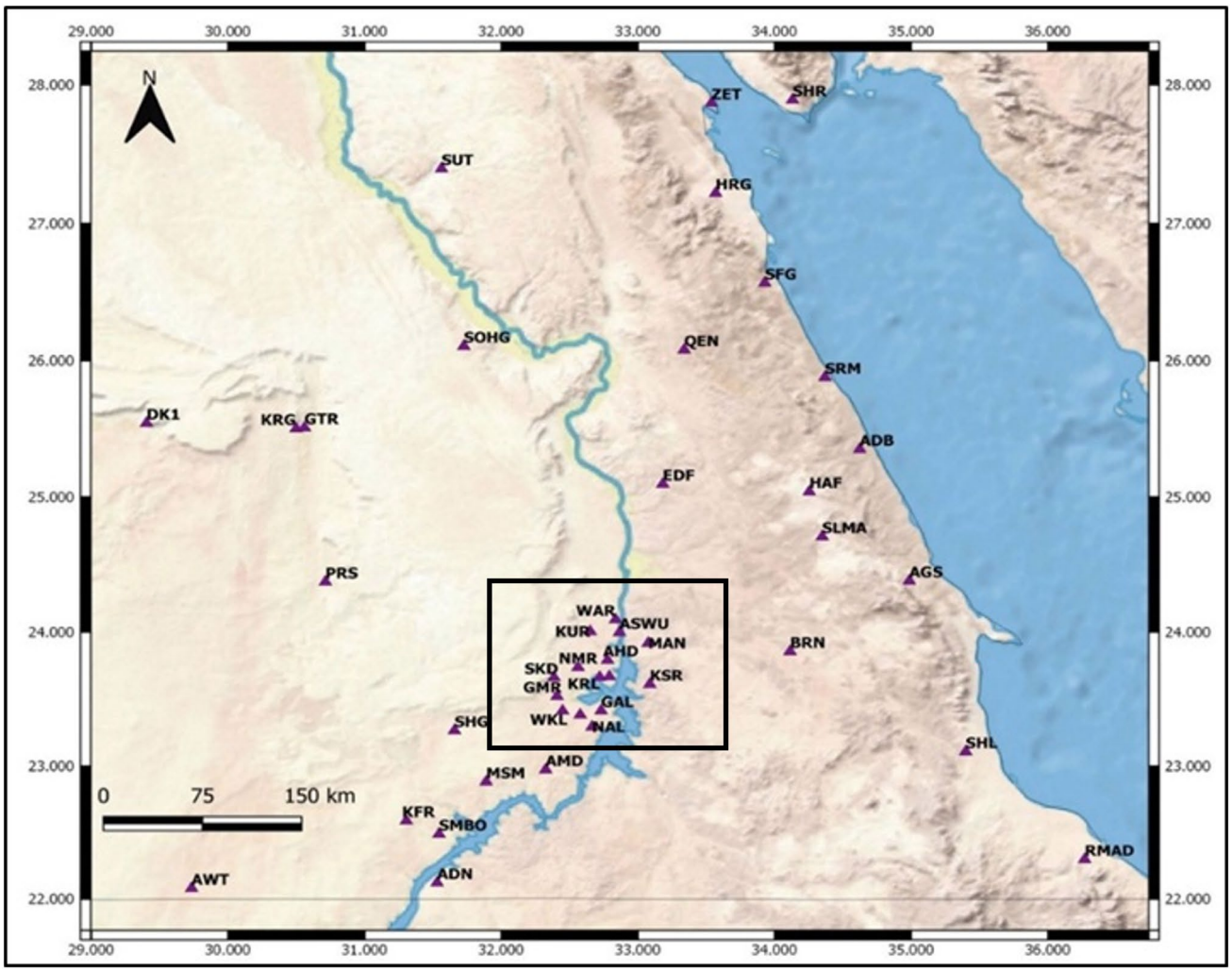

Fig. 6 Egyptian Seismic Stations south of Egypt including Aswan local Seismic network (inside the black square)

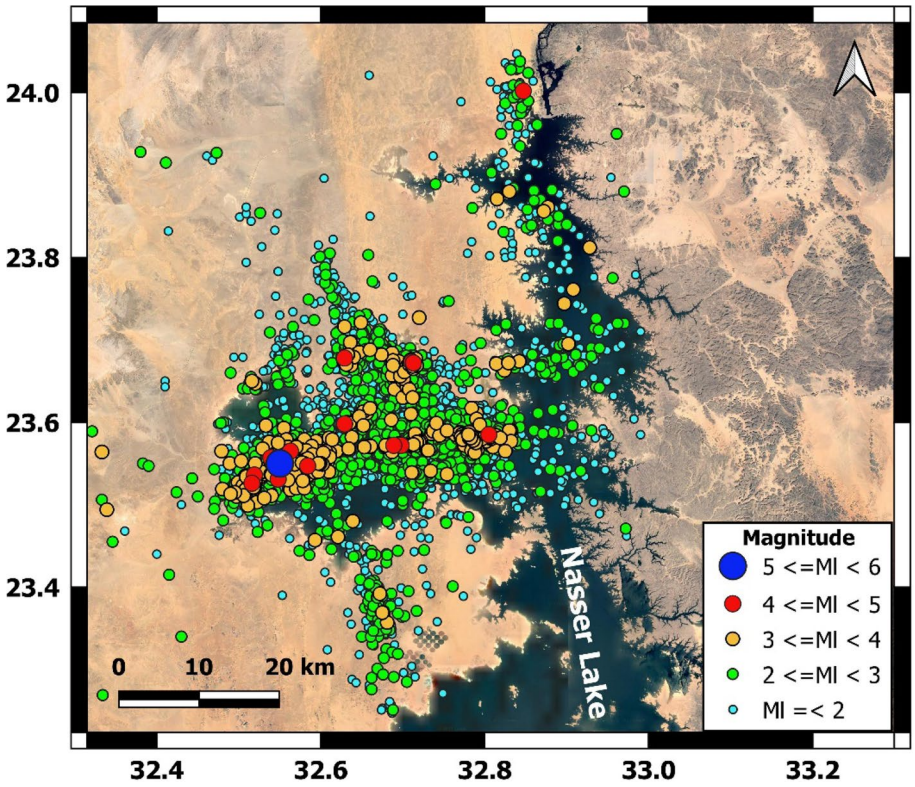

Fig. 7 Seismic activity at the northern part of Nasser Lake (1900–2022)

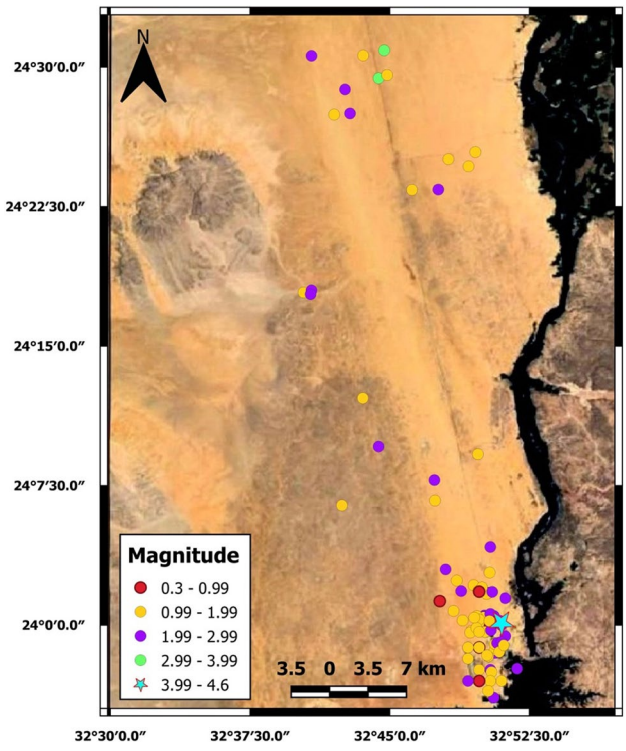

Fig. 8 Seismicity along the emergency spillway fault extension (1982–2022)

relationship between the number of earthquakes and the associated magnitudes as illustrated in Fig. 10. The two figures reveal probability of an increase and repetition of shallow earthquakes with small to moderate magnitude.

The seismic catalogue of the research region has been subjected to certain statistical analysis approaches using the ZMAP program (Malone and Wiemer 2001). The event magnitude in these dataset ranges from 0.5 to 4.6 with an exponential decrease in their numbers from low to high magnitudes (Fig. 10a). In Fig. 10b, the dataset's earthquake depth distribution is displayed. Figure 10c depicts the growth of the data set's seismic activity rate, or the total number of earthquakes projected against time. The frequency–magnitude relationship of earthquakes (log N = a − b M) was defined by Gutenberg and Richter (1956), where N is the number of earthquakes in various magnitude classes and a and b are constants. The b-value can be computed utilizing the maximum likelihood approach of Aki (1965):

$$b = \frac{1}{\ln 10\left(\left(\acute{M}\right) - M_{min}\right)}, \tag{1}$$

where $\acute{M}$ is the average magnitude and M_{min} is the smallest considered magnitude, the above equation characterizes the statistical behavior of the seismic activity in energy domain by using the frequency–magnitude distribution of earthquakes. The estimated b-value is 0.68 for the emergency

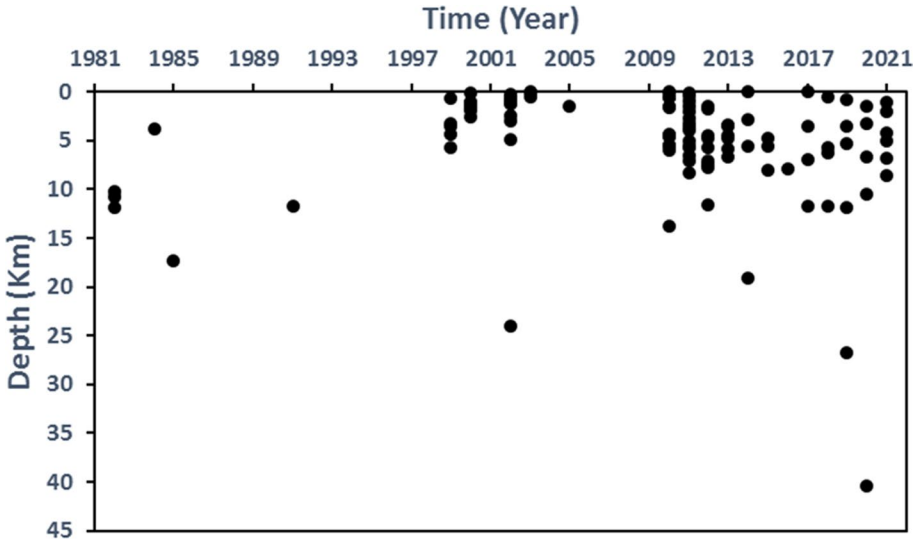

Fig. 9 Focal depth cross-section of the selected earthquakes along the emergency spillway fault (1982–2022)

spillway fault area, and the linear fitting of the distribution appears for M > 1.8 events (Fig. 10d).

In the Aswan seismic zones, the fault plane solution approach (Focal Mechanism) was utilized to determine the fault parameters for the active portions of the Kalabsha, Seiyal, and Abo Dirwa faults (Hassib 1990; Awad 1994; Badreldin et al. 2019). The polarities of the initial P-wave motion of the main shock and its aftershocks which recorded by Aswan seismic network have been used to estimate the composite focal mechanism of the seismic events locate along the emergency spillway fault (Fig. 11). Numerous studies have been published on the seismicity along active faults all over the world to display the focal source mechanism (Kürçer et al. 2008; Görgün and Albora 2017; Gorgun et al. 2020; Saadalla and Hamed 2022). Suetsugu program (Suetsugu 1995) has been used to plot the collected data on the lower focal hemisphere (Saadalla and Hamed 2022).

Moreover, the possibility of Nasser lake triggering of earthquakes that accompany the impoundment of major reservoirs was investigated by many author (e.g. Simpson et al. 1989; Hassib 1990; Mekkawi et al. 2004 and Gahalaut and Hassoup 2012). The increased vertical stress or loading and increasing pore pressure are two phenomena that alters the stress regime during filling huge reservoirs. In a few instances, seismic activity caused by reservoirs has been seen immediately after filling. Numerous studies have demonstrated a relationship between Nasser Lake's water level oscillations and the temporal distribution of seismicity. Obviously, Nasser Lake's water level is subject to a yearly cycle of change (Kebeasy and Gharib 1991; Hassib 1990; Awad 2002; Mekkawi et al. 2004). The water level typically reaches its high point in December and its lowest in August. Figure 12 displays daily distribution histograms of the seismic activity along the emergency spillway fault and lake water level for the time frame (1981–2021).

Aeromagnetic data

The Western Geophysical Company of America's Aero-Service Division conducted an airborne magnetic survey as part of an Egyptian-American joint effort to identify investment opportunities for mineral, petroleum, and groundwater resources in Egypt. The survey mainly focused on the Eastern Desert of Egypt and used the Varian V-85 proton magnetometer to gather magnetic data along NE-SW lines with a 1.5 km interval and a 93 m sampling interval along each profile. The aircraft also flew NW–SE lines at 10 km intervals perpendicular to the main flight lines and was limited to a minimum altitude of 120 m due to safety reasons. The Bendix Doppler Radar system was used to control the flight path, and diurnal magnetic field variations were recorded using a Varian VIW 2321 GA single-cell cesium vapor magnetometer. The magnetic data was corrected for diurnal variations and presented in the form of total magnetic intensity (TMI) data (Fig. 13).

The analysis of magnetic data is crucial for visualizing subsurface magnetic structures, especially the basement rocks. The qualitative interpretation of magnetic data provides a general view of the magnetic anomalies present on the magnetic map and the properties of their underlying sources. It typically begins with a visual examination of the magnetic anomalies. On the other hand, the quantitative interpretation deals with the forward modeling and

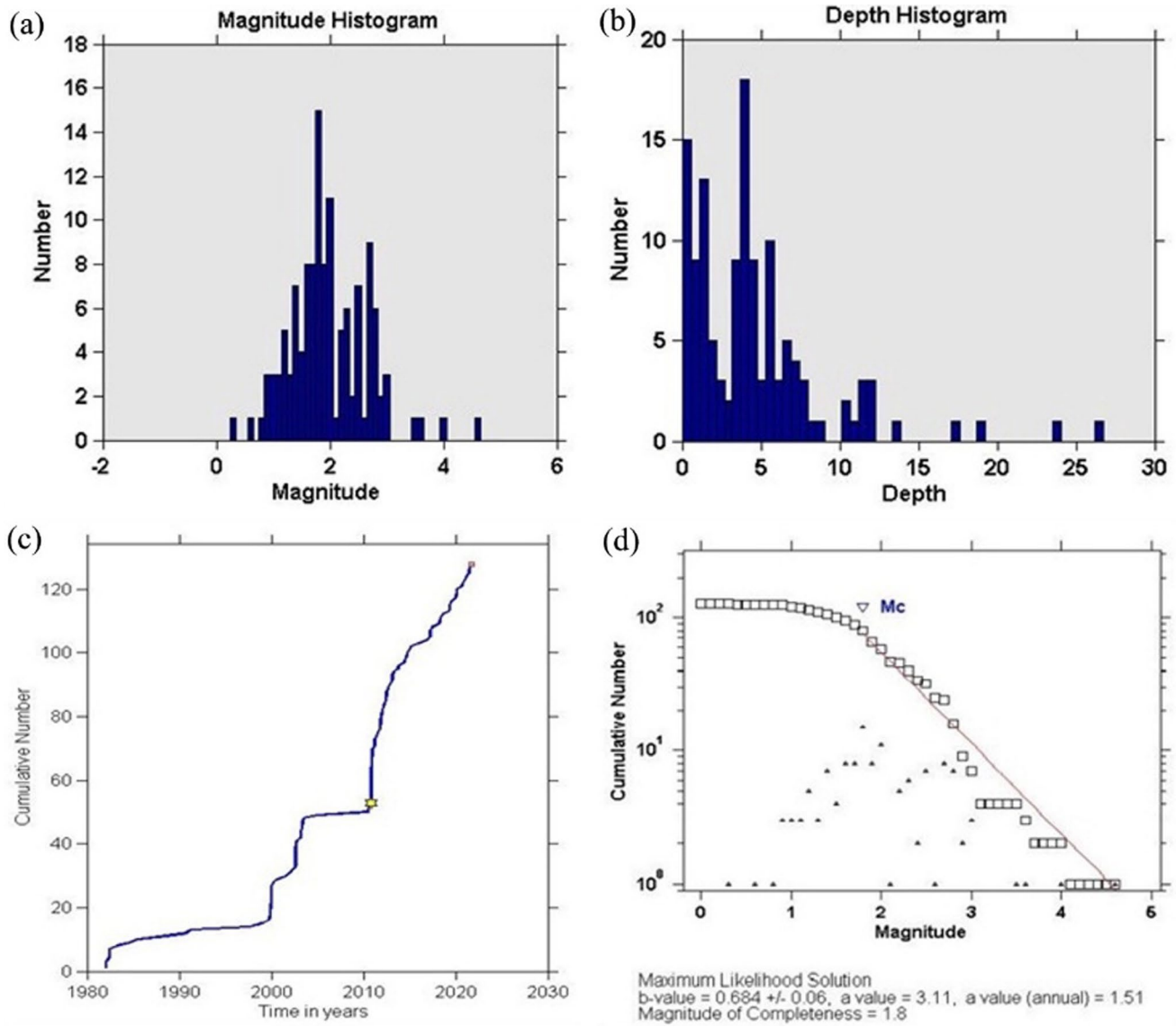

Fig. 10 **a** Histogram of magnitude distribution of the study dataset; **b** histogram of the depth distribution of the study dataset; **c** the cumulative number of earthquakes showing the level of seismic activity in data set; **d** the parameter b-value of the frequency–magnitude relationship

inversion of magnetic data, as well as determining the depth of the crystalline basement (Ghazala et al. 2018; Abuelnaga et al. 2020). Sedimentary rocks, which do not contain iron ores or basic intrusions, are typically non-magnetic, while metamorphic and igneous rocks are highly magnetized (Hrouda et al. 2009). As a result, the thickness of sedimentary rocks can be estimated by determining the depths to the magnetic sources (i.e., basement rocks) in the study area (Reeves 2005). The magnetic grid data underwent multiple analytical techniques with the aim of determining the subsurface structure of the study area (especially delineating the active emergency spillway fault). These techniques included reduction to the pole, regional-residual separation using the power spectrum method, filtering, depth estimation, tectonic trend analysis, and both forward and inverse modeling.

RTP of magnetic data

The magnetic intensity anomaly map of the area under investigation was created by gridding the magnetic data (Fig. 13). The magnetic field's undesirable distortion in the size, location, and shape of magnetic anomalies was eliminated by reducing the magnetic data to the North

Fig. 11 Focal mechanism for the November 7, 2010 earthquake

Magnetic Pole using Fast Fourier Transform and assuming only induced magnetization. This repositioned the anomalies above their sources. The magnetic data were reduced using mean values of 32.8° for inclination, 1.9° for declination, and 42,425 nT for the total magnetic field. As a result, the peaks in the RTP magnetic map (Fig. 14) almost align with the center of the magnetic bodies, and the asymmetry of the magnetic anomalies accurately reflects their true dips.

Regional-residual separation

In this study, we used the Geosoft software to detect lineation deduced from structural faulting in basement rocks at various depths using 2-D filtering applied to RTP aeromagnetic map (Oasis Montaj 2014). The cutoff number was set at 0.088 cycle/unit because it was appropriate for the depth in the area being analyzed on the aeromagnetic map (Fig. 15). In this work, two types of filters are used: residual (high-pass) (Fig. 16) and regional (low-pass) (Fig. 17). Long wavelengths pass through the low-pass filter, while wavelengths

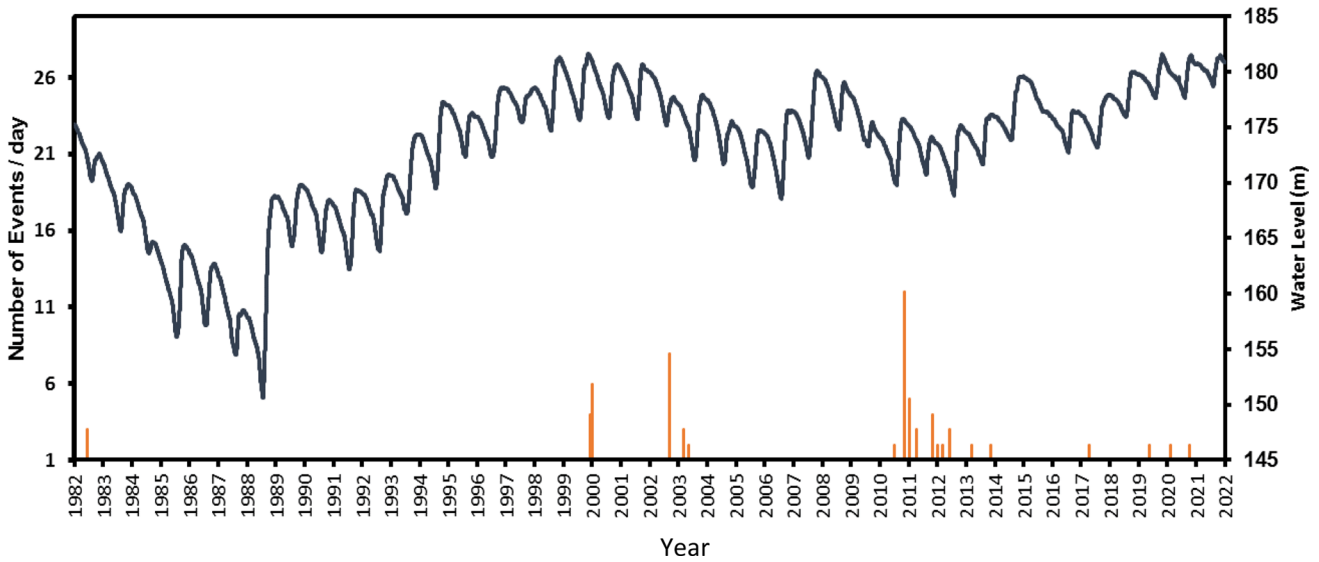

Fig. 12 Temporal variation in water level in Nasser Lake and earthquake activity along emergency spillway fault, during period (1982–2021)

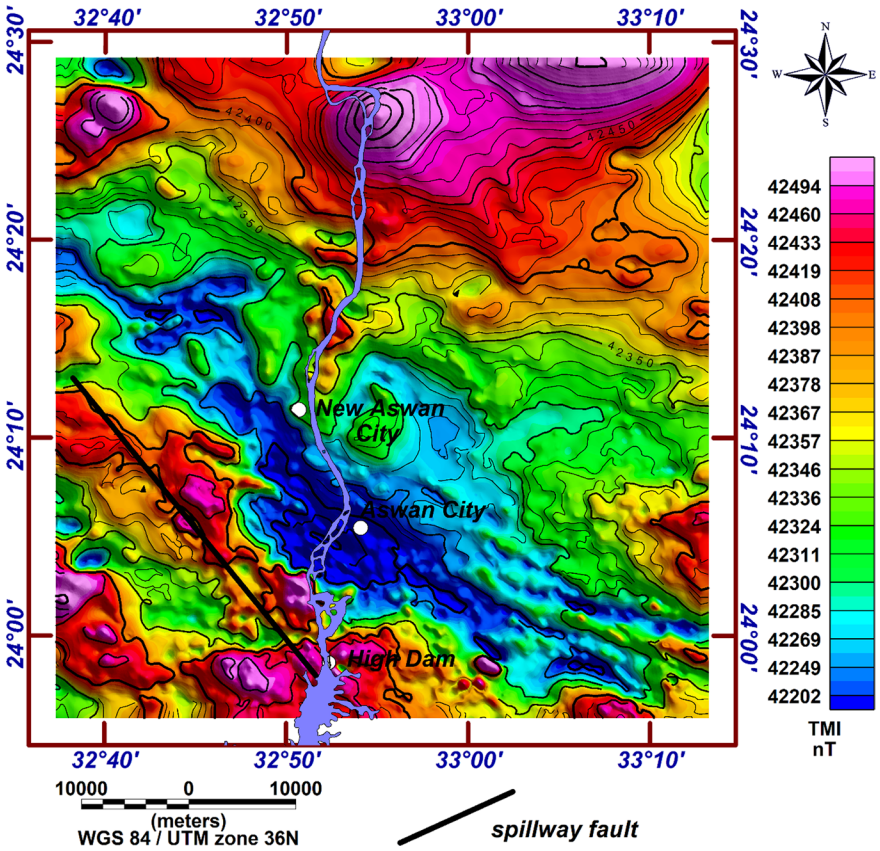

Fig. 13 TMI aeromagnetic anomaly map of the area of study with tracing of spillway fault

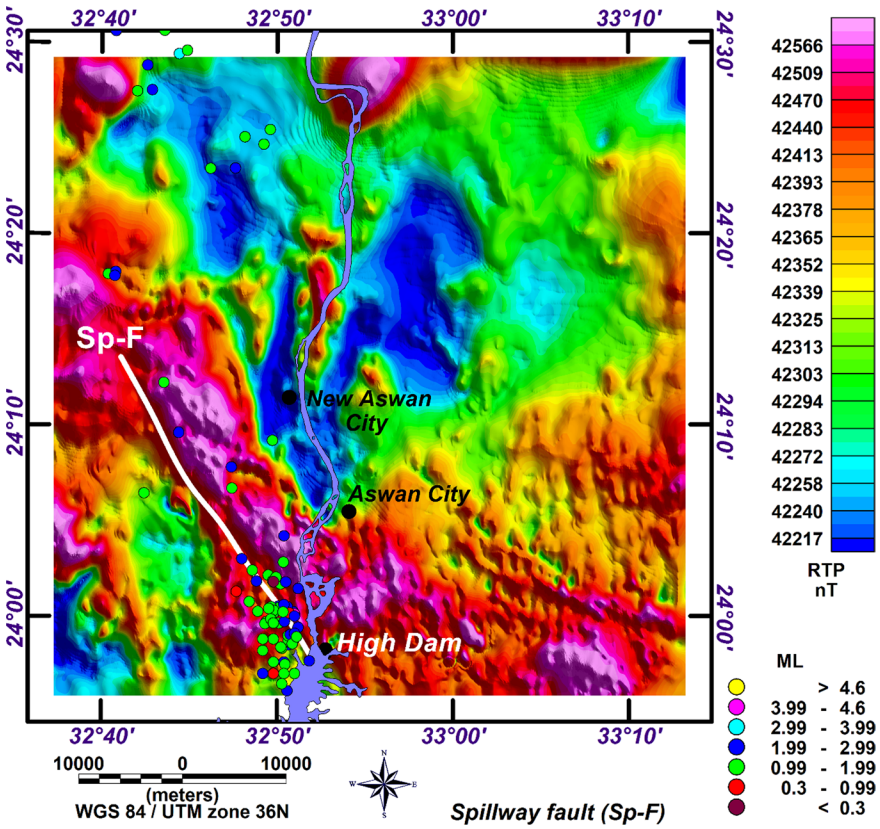

Fig. 14 RTP aeromagnetic anomaly map of the area of study with earthquake epicenters

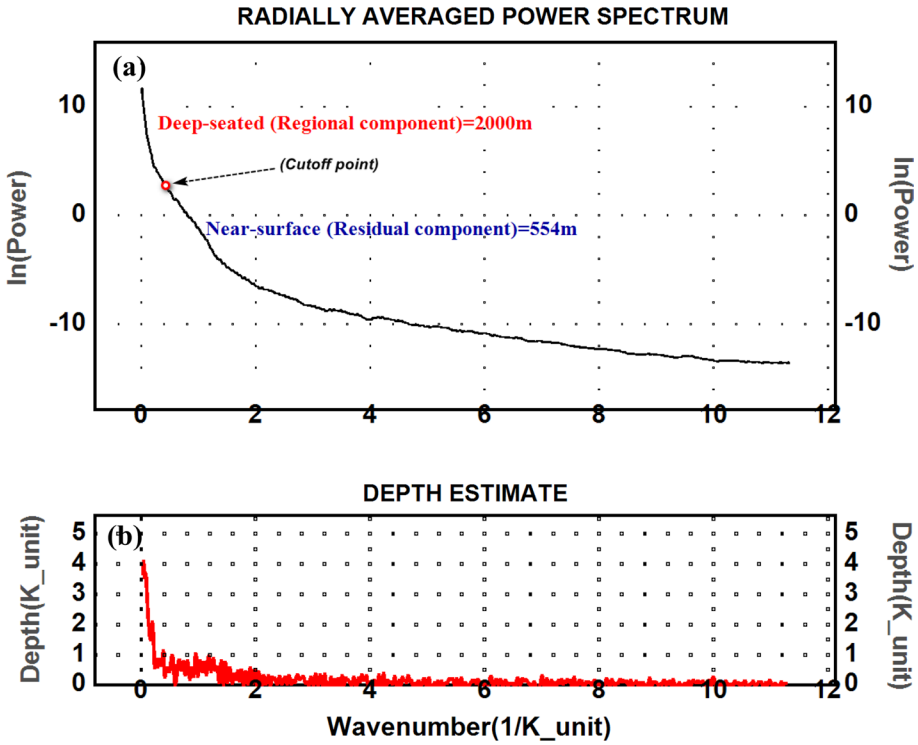

Fig. 15 2D radially averaged power spectrum of the aeromagnetic for the study area

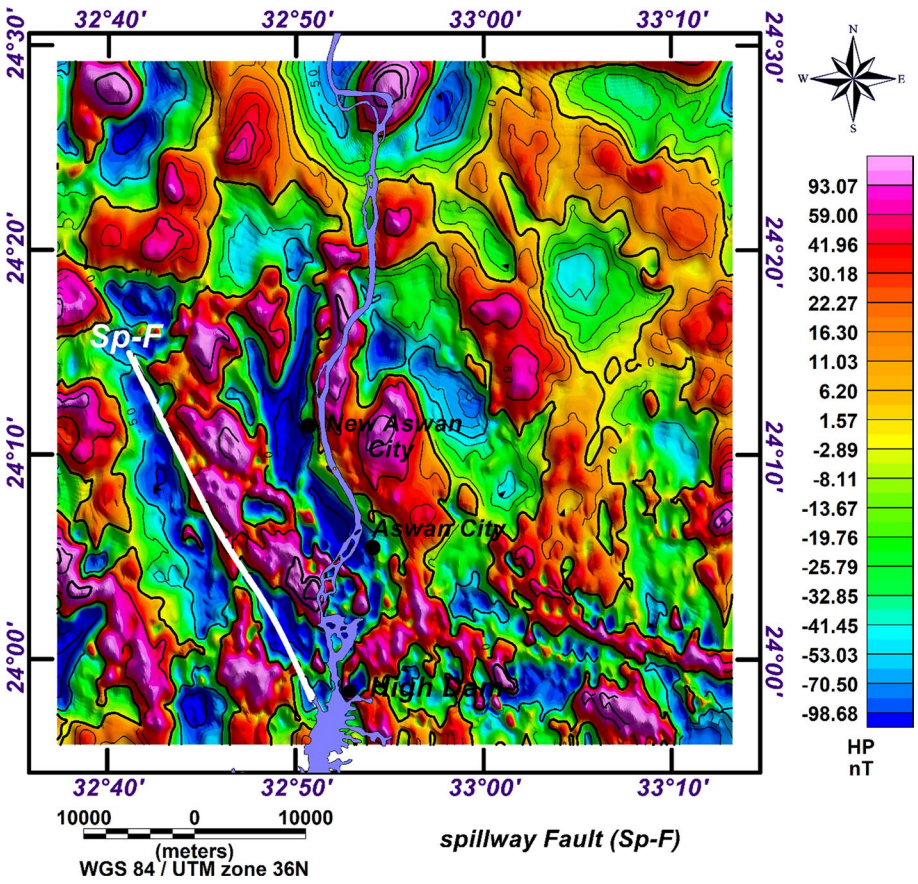

Fig. 16 High pass filtered RTP aeromagnetic map

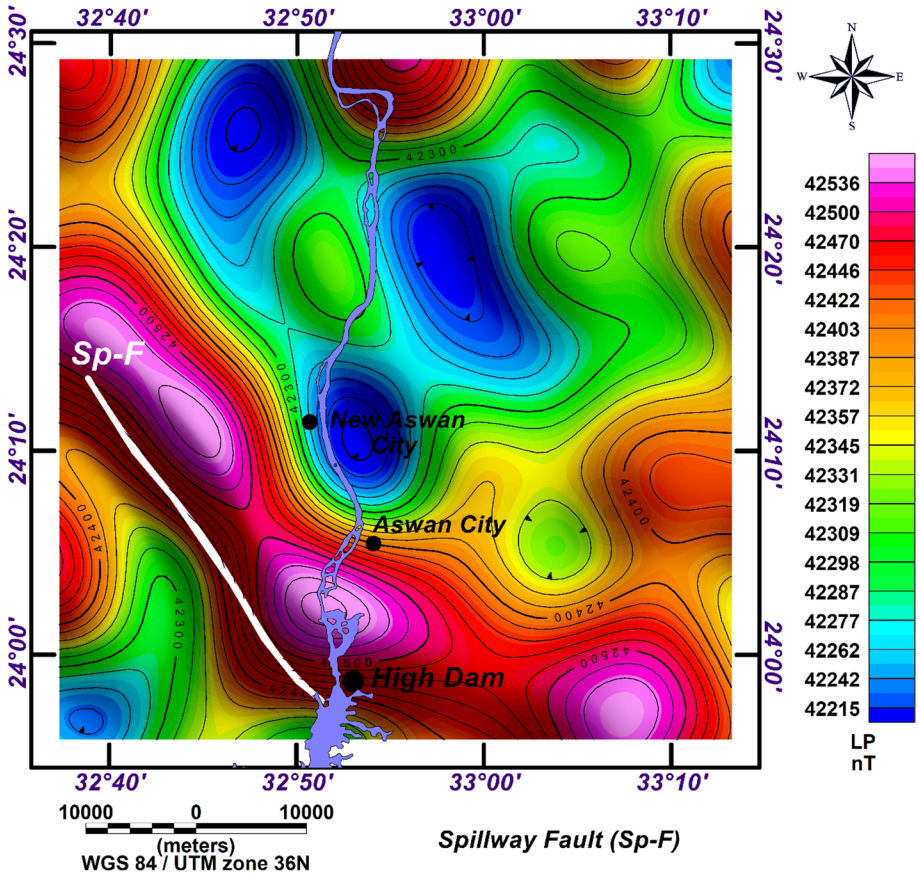

Fig. 17 Low pass filtered RTP aeromagnetic map

less than the cutoff wavelength are rejected, whereas the high-pass filter emphasizes short wavelengths while removing wavelengths greater than the cutoff wavelength (Torgow and Lubell 1964).

Euler deconvolution (ED)

By evaluating possible magnetic data, this approach might be utilized to establish the depth to the contact surface between sedimentary and basement rocks. It was primarily determined by magnetic data level, the structural index, and sampling rate. Furthermore, it is critical to comprehend the subsurface geology (Thompson 1982; Reid et al. 1990). When a background field's base level is taken into account, Euler's homogeneity equation may be stated as:

$$(x - x_0)\frac{df}{dx} + (y - y_0)\frac{df}{dy} + (z - z_0)\frac{df}{dz} = NF, \quad (2)$$

where the homogeneous function f is the observed field at location (x, y, z), which is caused by a source at location $(x_0; y_0; z_0)$, and N, physically, is a measure of the rate of decay of the field with the distance and, geophysically, is the structural index (SI) that is related directly to the shape of the causative source.

This technique studied by different authors Stravrev and Reid (2010), Gerovska and Araúzo-Bravo (2003), Gobashy and Al-Garni (2008), Abdelazeem and Gobashy (2016) and Abdelazeem et al. (2019). We used this technique to analyze RTP (aeromagnetic data), concentrating on the calculated depths and structural indices defined by distinct clusters that occurred from the various phases and utilizing them to determine the link between both the lineation that occurred and the geological units in the research region.

Depth estimates of isolated anomalies using the spectral analysis approach

Several authors (ex. Solovyev 1962; Bhattacarrya 1966; Spector and Grant 1970; Garcia and Ness 1994; Maurizio et al. 1998), demonstrated how to compute the average

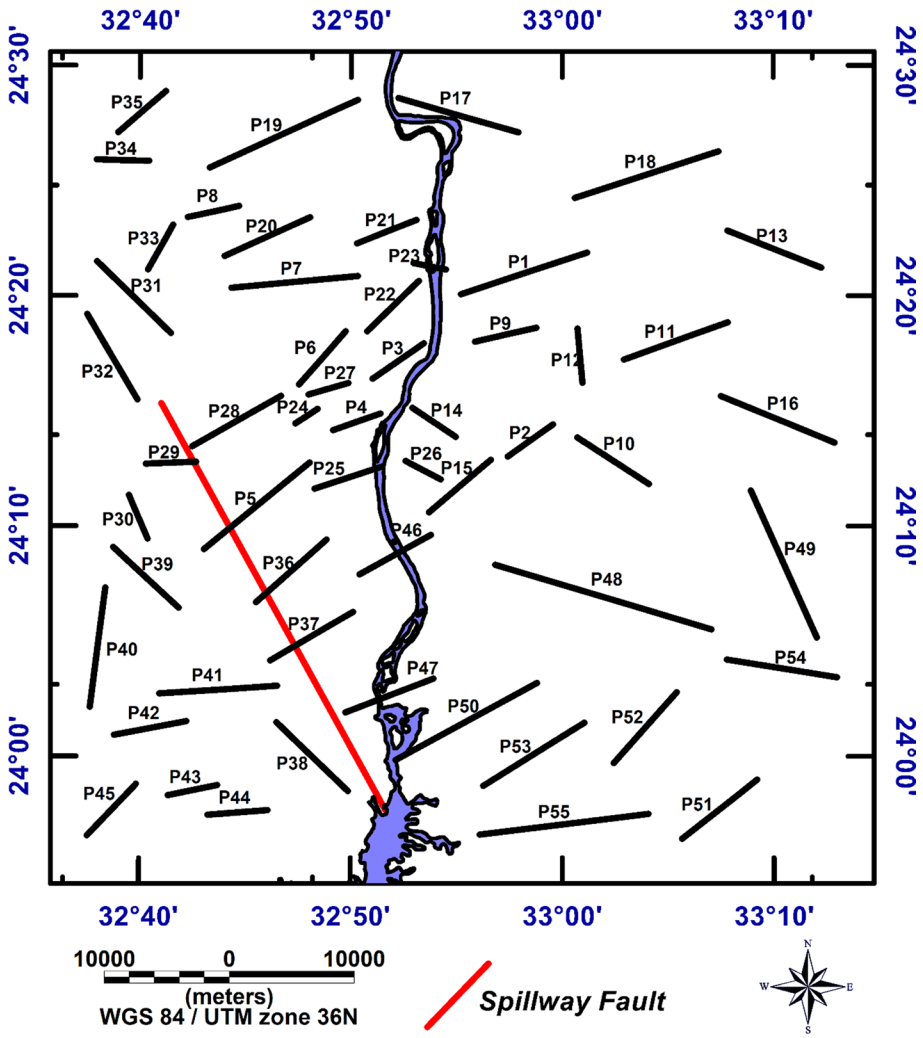

Fig. 18 Location map of the selected profiles for the basement depth estimation from the RTP aeromagnetic map using spectral analysis technique

depth levels to magnetic sources using spectrum analysis. Figure 18 shows the location of the selected magnetic anomalies (55 anomaly profiles were chosen from the RTP aeromagnetic map). Figure 19 shows an example of interpreted profiles.

Results and discussion

The obtained seismic database was used to construct the seismicity map for the study area. Obviously, the earthquakes' epicenters are scattered along the NW and SE direction. In Fig. 10c, It is interesting to observe that the number of earthquakes has increased through three phases: phase I, which occurred from 1982 to 1998, was marked by very low earthquake activity; while phase II appeared from 1998 to 2010 and marked by an increase in seismicity level due to the rising water level in Nasser Lake; the last one (phase III), which began with an earthquake of magnitude 4.6 in November 7, 2010 and continues even today with a relatively high rate of earthquake number. On the other hand, the low value of parameter b of the frequency–magnitude relationship has been attributed to the prevailing of shallow and small earthquakes as seen in Fig. 10d (Mogi 1967; Wiemer and Benoît 1996; Wiemer et al. 1998). The conditions can provide important constraints for analyzing the seismotectonic and hazard potential of a certain region (Malone and Wiemer 2001).

Furthermore, the combined fault plane solution for the November 2010 earthquake shows a normal fault with a small strike-slip component (Fig. 11). Therefore, the obtained fault trend by the current study and the trend of the listed trace by HADA and Soviet geologists, as well as the observed traces by satellite image, are identical. Consequently, the fault plane trend of the emergency spillway fault is the plane that takes NW–SE direction.

Gahalaut and Hassoup (2012) quantify the effect of the reservoir impoundment on the seismicity of the Aswan area, they calculated changes in stress and pore pressure due to the reservoir impoundment using Green's function approach, they concluded that pore pressure due to the fluid diffusion process from the reservoir might have played a very important role in the seismicity in the Aswan lake region due to reservoir impoundment. Hence, the Aswan seismicity is distributed on various faults with varying depths from 0 to 30 km, as pore pressure is the main causative factor, which includes fluid diffusion process. In the current study, from the available limited data, it appears that before 1998, the seismicity level of the emergency spillway fault more or less rare, but from November 2010 the largest event of the area ($M_L = 4.6$) occurred and the seismicity continues even today (Figs. 8, 9, 10). This observation, commensurable with the water filling history of the area (Fig. 12), strengthens our view that the pore pressure along with the contributions due to mass transfer of water from the reservoir into the sandstone played a main role in triggering the seismicity in the area of the emergency spillway fault. Zedan et al. (2002) and Fassieh et al. (2014) stated that during the years 1996–2000, water levels in Nasser Lake reservoir reached high values: 178.54 m (in November 1996) and 181.19 m (in November 1998). This water movement made the whole area fully saturated for the first time since the impoundment of the reservoir that began in 1964. Accordingly, the pore pressure in the region started building up in 1998, and was maximum for the first time in 2010, which ultimately led to the onset of seismicity in November 2010 and continues even today. Furthermore, Gahalaut and Hassoup (2012)

Table 1 The estimated basement depth values along the selected RTP magnetic anomaly profiles, using the spectral analysis technique

Profile no	Depth (m)	Profile no	Depth(m)	Profile no	Depth (m)
P-1	− 1590	P-21	− 442	P-41	− 430
P-2	− 2000	P-22	− 122	P-42	− 78
P-3	− 300	P-23	− 1190	P-43	− 95
P-4	− 1190	P-24	− 600	P-44	− 1193
P-5	− 600	P-25	− 1500	P-45	− 1989
P-6	− 140	P-26	− 1190	P-46	− 1989
P-7	− 1190	P-27	− 200	P-47	− 99
P-8	− 104	P-28	− 132	P-48	− 119
P-9	− 1600	P-29	− 99	P-49	− 91
P-10	− 440	P-30	− 99	P-50	− 99
P-11	− 1190	P-31	− 85	P-51	− 72
P-12	− 434	P-32	− 85	P-52	− 880
P-13	− 200	P-33	− 132	P-53	− 99
P-14	− 2900	P-34	− 100	P-54	− 104
P-15	− 106	P-35	− 75	P-55	− 149
P-16	− 126	P-36	− 700		
P-17	− 70	P-37	− 600		
P-18	− 150	P-38	− 300		
P-19	− 1421	P-39	− 140		
P-20	− 1060	P-40	− 119		

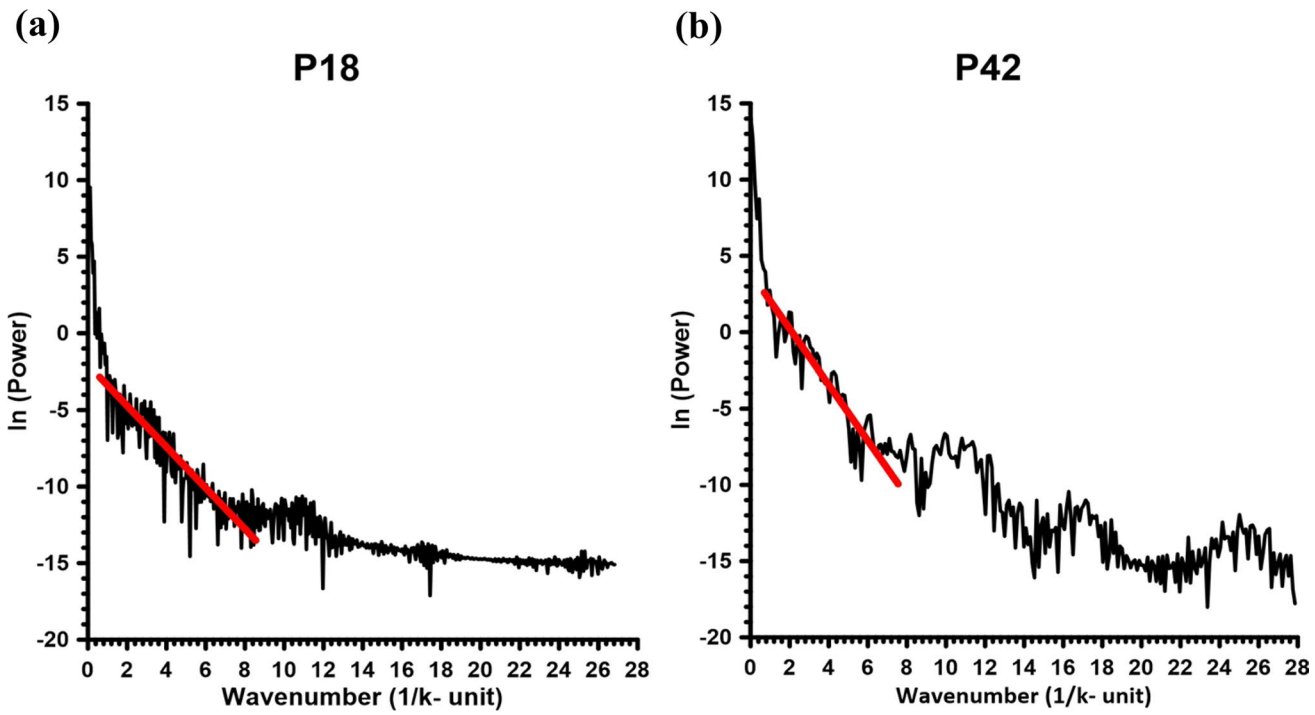

Fig. 19 Examples of the basement depth calculation along selected RTP aeromagnetic anomaly profiles using the spectral analysis technique

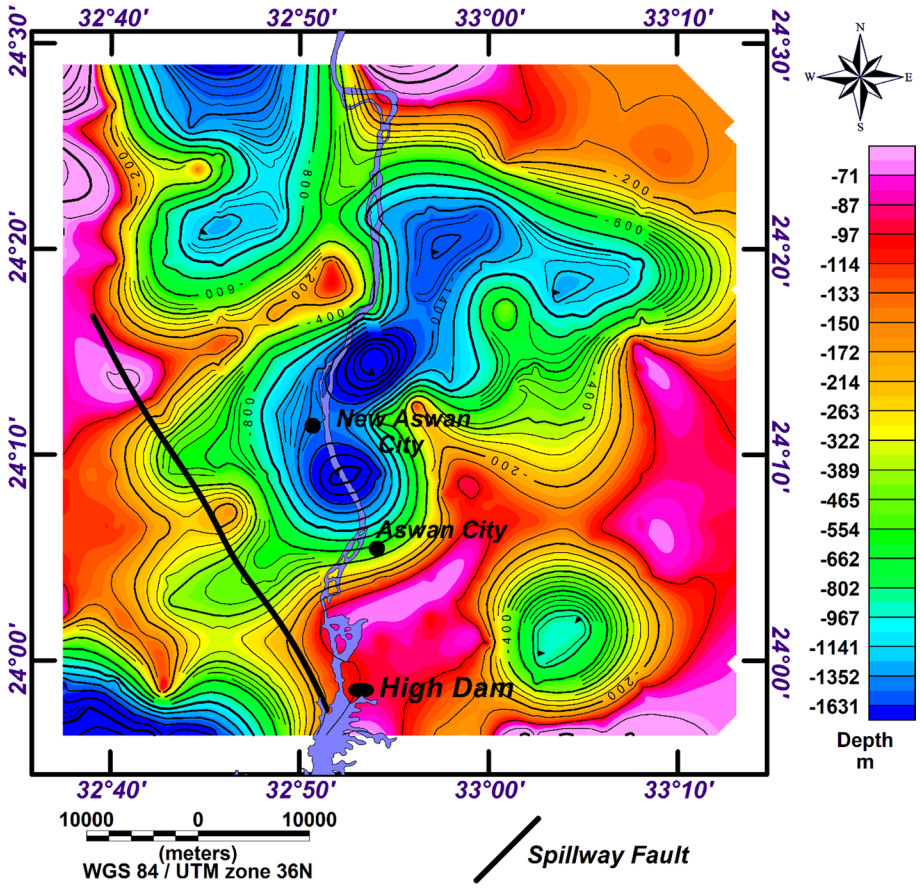

Fig. 20 Basement depth map in the studied area estimated by the spectral analysis technique

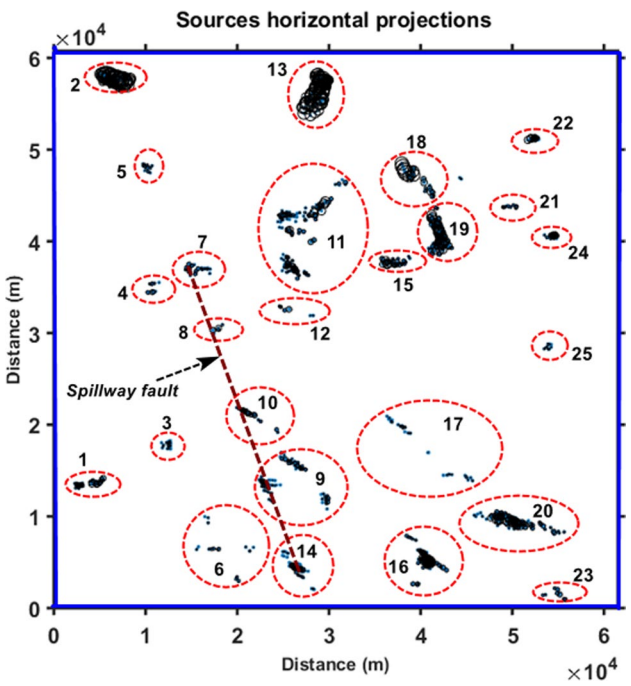

Fig. 21 Source horizontal projections of the accepted solutions

and Mekkawi et al. (2004) stated that the high pore pressure at shallower depth was enough to destabilize the faults for a longer period through small magnitude earthquakes. Also, it is notable that the periods 2000, 2003, and 2010 preceded by increasing in water level in the lake, and show a considerable increase in earthquake numbers.

The obtained aeromagnetic data shows that the southern, western, and southwestern parts of the region have the highest anomaly values, according to the RTP aeromagnetic anomaly map (Fig. 14), which has been prepared by modern computer programs. Low anomaly closures are clustered in the map's north, center, and northwest regions. A deep sedimentary basin is revealed by these anomalies. The area's highest anomaly is erratic, with high polarity varying from 42,370 to 42,580 nT. The processing of the magnetic data reveals frequent magnetic tendencies such as NW–SE, NE–SW, EW, and NS. This outcome is consistent with Abdelazeem et al. (2014). Earthquake epicenters and aeromagnetic data have been displayed in Fig. 14. It is evident that the seismic events follow the Emergency Spillway Fault trend that has been identified in the current study by the magnetic technique. As a result, our investigation revealed that the emergency spillway

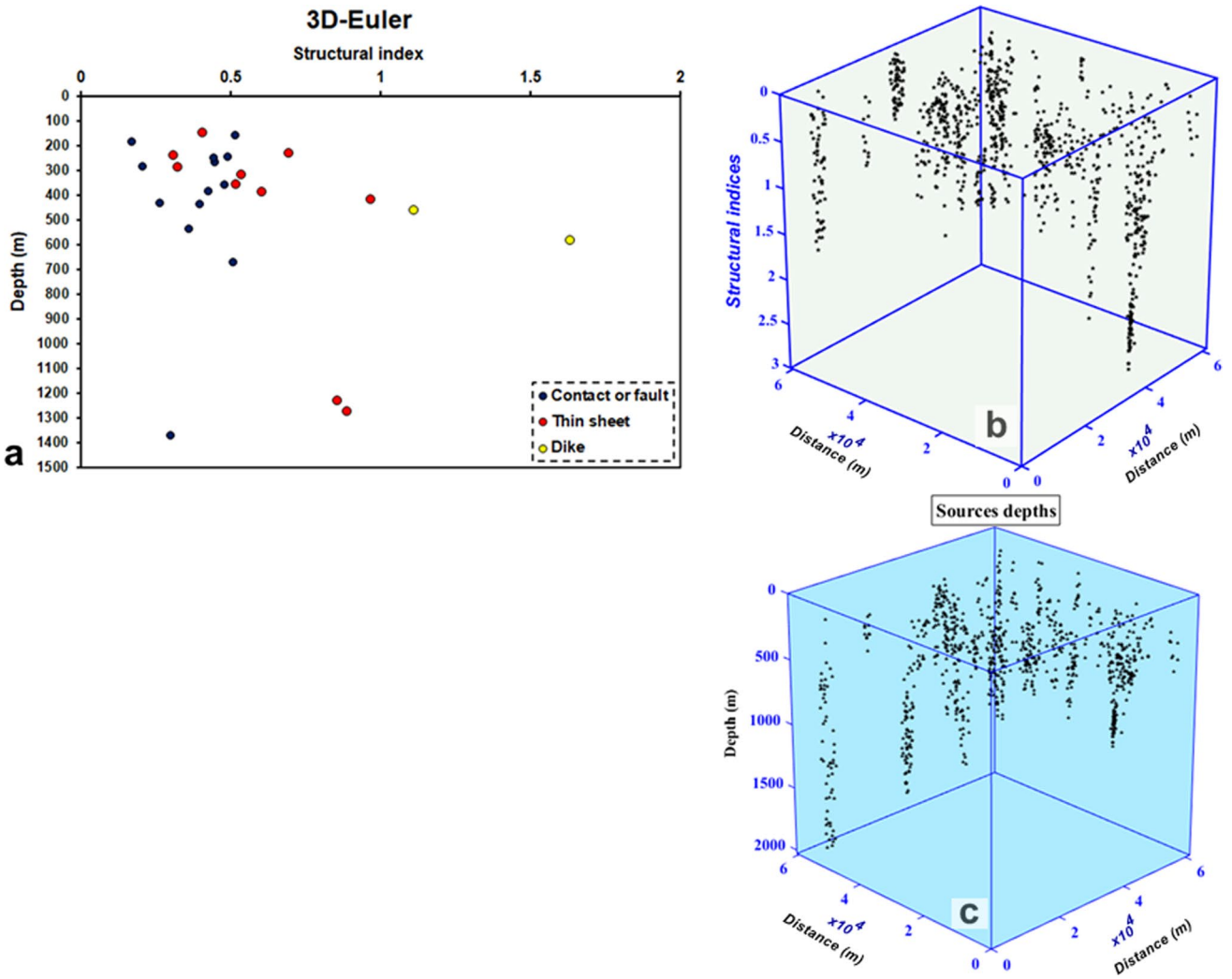

Fig. 22 **a** Scattered points between structural index and structural depth, **b** calculated structural indices of Euler solutions and **c** source depths of Euler solutions

fault extends from the northwestern corner of the region to the central portion of the southern half. The fault is prominently depicted in the magnetic maps, as evidenced by the elongation of contour lines and the high intensity of magnetic anomalies, which accurately depict the fault's location. The least valued location is in the northwest, with a magnetic anomaly of around 42,217 nT, while the magnetic abnormalities surrounding the High Dam reach a high of 42,556 nT. The area around the High Dam is also marked by positive and high-value magnetic anomalies, which are the result of the basement rocks' intensive tectonic activity. Because of the tectonic activity of the emergency spillway extension fault, whose southern section is located near the High Dam, and therefore poses a long-term seismic hazard to the High Dam site, these findings must be taken into account when estimating the seismic hazard for the Dam's site. The New Aswan City, on the other hand, is surrounded by heavy sediments that may assist in seismic wave amplification. As a result, an additional independent in-situ seismic geotechnical evaluation study has been conducted to examine the site effect of the New Aswan City's site.

On the other hand, on the RTP aeromagnetic map, wavelength filtering techniques, including 2D filtering, were employed to identify lineation deduced from structural faulting in basement rocks at various depths. Low-pass and high-pass filters are used in the research. The primary structural trend obtained from the residual magnetic processed map (Fig. 16) suggests that shallow structures with N–S, NW–SE and NE–SW alignments drive

Table 2 Results of Euler deconvolution analysis for the study area

Cluster	NumPoi	X_{avg}	X_{con}	Y_{avg}	Y_{con}	Z_{avg}	Z_{con}	SI_{avg}	SI_{con}
1	25	13,556.17	523.14	3604.49	2255.17	433.08	263.79	0.26	0.36
2	56	57,667.25	800.89	6477.30	1725.19	1275.63	982.30	0.89	0.95
3	16	17,830.10	647.61	12,428.26	675.19	158.24	154.57	0.51	0.47
4	8	34,944.64	1178.66	10,813.16	884.35	320.89	379.45	0.54	0.72
5	11	48,043.05	718.91	10,141.37	739.34	266.09	175.17	0.45	0.58
6	16	6462.19	4425.72	18,309.75	4355.42	242.70	233.96	0.31	0.48
7	19	36,952.07	666.96	15,667.46	1900.41	290.48	272.54	0.32	0.45
8	5	30,407.54	948.79	17,800.10	1164.84	390.05	672.58	0.61	1.10
9	69	14,131.40	3590.64	25,327.58	4708.26	252.04	260.18	0.44	0.63
10	19	21,348.76	825.52	21,007.92	1509.69	361.07	304.62	0.48	0.56
11	34	42,748.14	561.11	26,013.58	2189.34	243.82	348.87	0.49	0.66
12	97	39,586.82	7199.23	26,929.39	3670.27	357.92	430.58	0.52	0.70
13	61	56,288.39	2420.35	28,783.01	1456.67	1370.62	470.31	0.30	0.40
14	50	4405.98	1861.16	26,500.81	1645.80	232.15	307.91	0.70	1.03
15	23	37,718.62	557.67	37,173.14	1856.84	538.38	451.13	0.36	0.50
16	103	5242.58	1765.52	40,595.94	1356.25	582.71	511.47	1.64	1.64
17	27	17,889.18	5607.12	39,992.55	6789.73	148.32	181.27	0.41	0.49
18	11	47,584.05	1106.02	38,632.85	1094.71	1230.78	798.79	0.86	0.78
19	78	41,424.43	4463.17	41,901.88	1477.72	670.62	549.50	0.51	0.59
20	80	9454.53	1125.13	50,156.56	4164.68	463.72	384.92	1.11	1.21
21	9	43,785.05	197.77	49,704.20	1203.38	284.70	290.21	0.21	0.34
22	18	51,228.24	256.34	52,435.91	685.08	435.59	578.90	0.40	0.50
23	8	1507.92	1028.50	54,747.05	2050.97	382.84	238.43	0.43	0.49
24	22	40,559.34	298.92	54,408.18	657.54	419.64	462.97	0.97	1.01
25	8	28,498.32	572.18	53,955.16	595.36	183.33	179.52	0.17	0.22

NumPoi, number of points; Xavg, average x value; Xcon, confidence interval for variable X; Yavg, average Y value; Ycon, confidence interval for variable Y; Zavg, average z value; Zcon, confidence interval for variable Z; SIavg, average estimated structural indices for each cluster; SIcon, confidence interval for estimated structural indices N

local structural trends. However, Gaber et al. (2011) found two groups of faults (E–W and NW–SE) derived from satellite data. As a result, the emergency spillway fault takes northwest to southeast directions, and the contour lines surrounding the main fault have extreme elongation and high gradation and defined by Koch et al. (2012). In agreement with Saleh (2011), the depth to the top of the basement rocks in the study area vary from 60 to greater than 1670 m (Table 1) and (Fig. 20). In order to assess the depth to the contact surface between sedimentary and basement rocks, the newly improved 2D Euler Deconvolution technique (ED) was deployed to calculate the position and the magnetic anomaly source depth. The solutions that have been approved are divided into 25 categories (Figs. 21, 22). Table 2 summarizes the clusters of solutions, their confidence and mean positions, as well as the indices of the structures. Table 3 shows the depths, structure indices, and structural shapes. The most prevalent structural element is represented by the cluster index G16 (103 points of solution). It has an average depth of 583 m and average structure index 1.6, assuming dike or sill. The predominant structural trends deduced from this technique are the NW–SE, and N–S directions.

So, we could say that in the current study the obtained seismic activity pattern along the west of the High Dam to Kom-Ombo city matches to the satellite image and the resulted maps from the aeromagnetic data and reflect in precisely the emergency spillway fault trend.

Conclusions

The present study aims to track the surface and subsurface path of the emergency spillway fault in order to update the current seismic source model for using in separated study for assessing the seismic hazard and risk on

Table 3 Average depths (Z_{avg}) in meters and structural indices (SI_{avg}) for different groups

Cluster	Z_{avg}	SI_{avg}	Predicted causative structure
G1	433.08	0.26413	Contact
G2	1275.63	0.89002	Contact/thin sheet
G3	158.238	0.51451	Contact
G4	320.889	0.53599	Contact/thin sheet
G5	266.086	0.44579	Contact
G6	242.7	0.31094	Contact/thin sheet
G7	290.476	0.32261	Contact/thin sheet
G8	390.054	0.60549	Contact/thin sheet
G9	252.044	0.4438	Contact
G10	361.073	0.47921	Contact
G11	243.815	0.49143	Contact
G12	357.918	0.51956	Contact/thin sheet
G13	1370.62	0.298	Contact
G14	232.151	0.69676	Contact/thin sheet
G15	538.379	0.36002	Contact
G16	582.71	1.63511	(Sill/dike)
G17	148.316	0.40592	Contact/thin sheet
G18	1230.78	0.85849	Contact/thin sheet
G19	670.624	0.5084	Contact
G20	463.718	1.11322	(Sill/dike)
G21	284.702	0.20629	Contact
G22	435.589	0.39541	Contact
G23	382.836	0.426	Contact
G24	419.64	0.97037	Contact/thin sheet
G25	183.331	0.17033	Contact

the High Dam and the new city of Aswan. The seismicity and aeromagnetic techniques have been applied together for achieving this goal. At first, the seismic database was processed to estimate the earthquake source parameters and create a seismicity map and graphs, which reveal the clustering of shallow seismic events with small magnitude along the geological fault trace. Moreover, the obtained focal mechanism solution for the main earthquake along the emergency spillway fault has been done. The pore pressure shows a specific role in activation process of the emergency spillway fault after the saturation of the shallower sandstone strata with water in 1998. On the other hand, the aeromagnetic data have been subjected to different kinds of processing and filtering, low and high pass filtered RTP aeromagnetic maps have been obtained for revealing the deep sedimentary basin, the processed aeromagnetic data reveals frequent magnetic tendencies most notably in northwest-southeast direction. The obtained results from both geophysical techniques showed that the fault trace runs from northwest to southeast and the obtained seismic activity pattern along the west of the High Dam highly matches the trend obtained from aeromagnetic data. Furthermore, the aeromagnetic results confirm that the fault is shallow and has normal down through combined slightly with small strike-slip component. A continuous monitoring of the earthquake activity that is associated with the emergency spillway fault is necessary to minimize its possible geo-hazardous effects on the High Dam and new Aswan city.

Acknowledgements High appreciation for the National Research Institute of Astronomy and Geophysics and his president for supporting and funding this research. Many thanks to the Aswan Regional Earthquake Research Center's researchers and technical team for their support in completing this study. Our deep thanks to the Associate Editor of Acta Geophysica Journal and anonymous reviewers for their valuable suggestions and comments which have greatly help to improve the manuscript.

Author contributions All of the authors contributed to the study's conception and design. Material preparation and data collection were handled by all authors. On the other hand, AH and MK contributed to data analysis and prepared the initial draught of the manuscript, and all authors provided comments on previous draughts. All authors reviewed and approved the final manuscript.

Funding Open access funding provided by The Science, Technology & Innovation Funding Authority (STDF) in cooperation with The Egyptian Knowledge Bank (EKB). This work has been funded by The National Research Institute of Astronomy and Geophysics (NRIAG) in Cairo, Egypt.

Declarations

Conflict of interest There are no relevant financial or non-financial concerns that the authors must declare. While, the funding come only from our institute (NRIAG) Cairo, Egypt.

References

Abbas MA, Fat-Helbary RE-S, Hamed A, El-Faragawy KO, El-Amin EM, El-Qady GM (2023) The implementation of shallow geophysical survey for detection of some buried archaeological structures in Aswan City, Egypt. Sustainable conservation of UNESCO and other heritage sites through proactive geosciences. Springer. https://doi.org/10.1007/978-3-031-13810-2_11

Abdelazeem M, Gobashy MM (2016) A solution to unexploded ordnance detection problem from its magnetic anomaly using Kaczmarz regularization. Interpretation 4(3):SH61–SH69

Abdelazeem MA, Mekkawi M, Gobashy M (2014) Subsurface structures using a new integrated geophysical analysis, South Aswan. Egypt Arab J Geosci 7(12):5141–5157

Abdelazeem M, Fathy MS, Khalifa MM (2019) Integrating magnetic and stratigraphic data to delineate the subsurface features in and around new Galala City, Northern Galala Plateau. Egypt NRIAG J Astron Geophys 8(1):131–143

Abuelnaga HS, Aboud E, Harbi HM, Alqahtani FA, Qaddah AA (2020) Delineating flood hazards using the interpreted structural setting and GIS in Attaif, western Saudi Arabia. Arab J Geosci 13:1–18

Aki K (1965) Maximum likelihood estimates of b-value in the formula log N = a – mb and its confidence limits. Bull Earthq Res Inst 43:237–239

Ambraseys NN, Melville CP, Adams RD (1994) The seismicity of Egypt. Cambridge University Press, Arabia and Red Sea

Awad H (2002) Seismicity and water level variations in the Lake Aswan area in Egypt 1982–1997. J Seismol 6:459–467

Awad H (1994) Investigation of the tectonic setting, seismic activity and crustal deformation in Aswan seismic region. Ph.D. thesis, Tokyo University, Egypt

Badreldin H, Abdel-Aal AA, Toni M, El-Faragawy K (2019) Moment tensor inversion of small-to-moderate size local earthquakes in Egypt. J Afr Earth Sci. https://doi.org/10.1016/j.jafrearsci.2018.12.004

Bhattacharyya BK (1966) Continuous spectrum of the total-magnetic-field anomaly due to a rectangular prismatic body. Geophysics 31(1):97–121

Dahy SA (2012) A study on shallow and deep focus earthquakes and relationship to the water level in the western side of the Aswan High Dam Lake Egypt. Res J Earth Sci 4(2):63–68. https://doi.org/10.5829/idosi.rjes.2012.4.2.6377

Dahy SA, Hassib GH, Mohamed AS (2009) Investigation of induced seismicity in the northwestern part of the Aswan High Dam Reservoir, Egypt. In: Sixth international conference on the geology of Africa, Assiut, Egypt, pp 24–26

EGSMA (The Egyptian Geological Survey and Mining Authority) (1981) Geologic map of Egypt: scale 1: 2000 000. Egyptian Geological Survey and Mining Authority, Cairo, Egypt

Fassieh KM, Zaki MA (2014) A water management model for Tushka depression. J Appl Math 2014:731846. https://doi.org/10.1155/2014/731846

Fat-Helbary RES, El-Faragawy KO, Hamed A (2019a) Soil geotechnical characteristics for seismic risk mitigation at the southern extension of Marsa Alam city, Egypt. NRIAG J Astron Geophys 8(1):1–14

Fat-Helbary RE-S, El-Faragawy KO, Hamed A (2019b) Application of HVSR technique in the site effects estimation at the south of Marsa Alam City, Egypt. J Afr Earth Sci 154(June 2019):89–100. https://doi.org/10.1016/j.jafrearsci.2019.03.015

Fat-helbary R, Haggag M (2004) Seismicity and seismotectonic of the west Kom Ombo area, Aswan, Egypt. Acta Geodyn Geomater 1(2):195–200

Gaber A, Koch M, Geriesh MH, Sato M (2011) SAR remote sensing of buried faults: implications for groundwater exploration in the Western Desert of Egypt. Sens Imaging Int J 12(3–4):133–151

Gahalaut K, Hassoup A (2012) Role of fluids in the earthquake occurrence around Aswan reservoir, Egypt. J Geophys Res 117:B02303. https://doi.org/10.1029/2011JB008796

Garcia-Abdeslem J, Ness GE (1994) Inversion of the power spectrum from magnetic anomalies. Geophysics 59(3):391–401

Geoshy MS, Mabrouk MA, Mousa SA, Abd El Nabi SH, Zarif FM (2020) Application of transient electromagnetic method (TEM) for groundwater exploration in El-Gallaba Plain, West of Kom Ombo, Upper Egypt. EGS J 18(1):123–132

Geosoft Program (Oasis Montaj) (2014) Aero Service Company, Mineral Petroleum Ground-Water Assessment Program (MAGMAP), 2-D Frequency-Domain Processing, Geosoft Inc., Toronto, Canada

Gerovska D, Araúzo-Bravo MJ (2003) Automatic interpretation of magnetic data based on Euler deconvolution with unprescribed structural index. Comput Geosci 29(8):949–960

Ghazala HH, Ibraheem IM, Haggag M, Lamees M (2018) An integrated approach to evaluate the possibility of urban development around Sohag Governorate, Egypt, using potential field data. Arab J Geosci 11:1–19

Gobashy MM, Al-Garni MA (2008) High resolution ground magnetic survey (HRGM) for determining the optimum location of subsurface dam in Wadi Nu'man, Makkah Al Mukarammah, KSA Earth Sci 19(1)

Görgün E, Albora AM (2017) Seismotectonic investigation of Biga peninsula in SW Marmara region using steerable filter technique, potential field data and recent seismicity. Pure Appl Geophys 174(10):3889–3904

Görgün E, Kalafat D, Kekovalı K (2020). Source mechanisms and stress field of the 2017 Ayvacık/Çanakkale earthquake sequence in NW Turkey. Ann Geophys 63(3)

Gutenberg B, Richter CF (1956) Magnitude and energy of earthquakes. Ann Geofis 9:1–15

Hamed A (2019) Seismic microzonation for earthquake risk mitigation at the southern extension of Marsa Alam City. Ph.D.'s Thesis, Aswan University, Aswan, Egypt

Hassib G (1990) A study on the earthquake mechanics around the High Dam Lake, Aswan, Egypt. Ph.D thesis, Faculty of Science, South Valley University, Sohag, Egypt

Hrouda F, Chlupacova M, Chadima M (2009) The use of magnetic susceptibility of rocks in geological exploration. Terraplus, Brno, 2016

Jeffrey DR (2011) Structural influence on the evolution of a pre-Eonil drainage system of southern Egypt: insights from magnetotellurics and gravity data. M.Sc. thesis, Oklahoma State University, USA, pp 1–67

Kebeasy RM, Gharib AA (1991) Active fault and water loading are important factors in triggering earthquake activity around Aswan Lake. J Geodyn 14:73–83

Kebeasy RMM, Maamoun EM, Ibrahim A, Megahed DS, Leith W (1987) Earthquake studies at Aswan reservoir. J Geodyn 7:173–193

Khalil AE, El-Hady SM, Hosny A (2004) Three-dimensional velocity structure of VP and VP/VS around Aswan area, Egypt. J Appl Geophys 3(1):303–314

Klein FW (1978) Hypocenter location program HYPOINVERSE. U. S. Geological Survey, Open-File Report. 78–694:102

Koch M, Gaber A, Burkholder B, Geriesh MH (2012) Development of new water resources in Egypt with earth observation data. Oppor Chall Int J 1(3):1–11

Kürçer A, Chatzipetros A, Tutkun SZ, Pavlides S, Ateş Ö, Valkaniotis S (2008) The Yenice-Gönen active fault (NW Turkey): active tectonics and palaeoseismology. Tectonophysics 453(1–4):263–275. https://doi.org/10.1016/j.tecto.2007.07.010

Maamoum M, Megahed A, Allam A (1984) Seismicity of Egypt. HIAG Bull IV (Ser. B), pp 109–160

Malone S, Wiemer S (2001) A software package to analyze seismicity: ZMAP. Seismol Res Lett 72:374–383

Maurizio F, Tatina Q, Angelo S (1998) Exploration of a lignite bearing in Northern Ireland, using ground magnetic. Geophysics 62(4):1143–1150

Mekkawi M, Grasso JR, Schnegg PA (2004) A long-lasting seismic relaxation of seismicity at Aswan reservoir, Egypt, 1982–2001. Bull Seismol Soc Am 94(2):479–492

Mekkawi M, Abdel Monem SM, Rayan A, Mahmoud SM, Saleh A, Moustafa S (2008) Subsurface tectonic structure and crustal deformation at kalabsha fault, Aswan-Egypt, from magnetic, GPS and seismic data. NRIAG J Geophys, Special issue, Helwan, Egypt

Merlina J, Radwan AH, Hassan R, Mahmoud SM, Tealeb AA, Issawy EA (2003) Temporal variations of gravity in the Aswan region, Egypt. J Geodyn 35(4–5):499–509

Mogi K (1967) Earthquakes and fractures. Tectonophysics 5:35–55

Primary Report on the November, 7, 2010 earthquake, North-West the High Dam (2011) Aswan Regional Earthquake Research Center (In Arabic)

Reeves C (2005) Aeromagnetic surveys: principles, practice and interpretation, vol 155. Geosoft, Washington (DC), p 2005

Reid AB, Allsop JM, Granser H, Millett AJ, Somerton IW (1990) Magnetic interpretation in three dimensions using Euler Deconvolution. Geophysics 55:80–90

Report No. 169 (1966) Geological engineering conditions of the emergency spillway area, p 19

Saadalla H, Hamed A (2022) Source characteristics of the 16 June 2020 ML 5.4 earthquake and its significant aftershock sequences, northern Red Sea, Egypt. Geosci Lett 9:41. https://doi.org/10.1186/s40562-022-00250-x

Said R (1962) The geology of Egypt. Elsevier Publishing Co., Amsterdam, p 377

Sakran S, Said SM (2018) Structural setting and kinematics of Nubian fault system, SE Western Desert, Egypt: an example of multi-reactivated intraplate strike-slip faults. J Struct Geol. https://doi.org/10.1016/j.jsg.2017.12.006

Saleh S (2011) Subsurface structural mapping of Northern Nasser Lake region, Aswan, Egypt, using Bouguer data. Contrib Geophys Geod 41(1):45–72

Simpson DW, Gharib AA, Kebeasy RM (1989) Induced seismicity and changes in water level at Aswan reservoir, Egypt. Gerlands Beitr Zur Geophys, Special issue on Induced Seismicity, Leipzig 99:191–204

Solovyev A (1962) Use of the frequency method for determination of some parameters magnetic body. IZV Akad NAUK SSSR Sibirkoye Ptedliye Geologyaa 2:122–125

Spector A, Grant FS (1970) Statistical models for interpreting aeromagnetic data. Geophysics 35:293–302

Stavrev P, Reid A (2010) Euler deconvolution of gravity anomalies from thick contact/fault structures with extended negative structural index. Geophysics 75(6):I51–I58

Suetsugu D (1995) Earthquake source mechanism, IISEE Lecture note. Tsukuba, Japan, pp 105

Thompson DT (1982) EULDPH—a technique for making computerassisted depth estimates from magnetic data. Geophysics 47:31–37

Torgow EN, Lubell PD (1964) Bandpass filters with steep skirt selectivity. In: PTGMTT international symposium digest, vol 64(1). IEEE, pp 22–26

Wiemer S, Benoit J (1996) Mapping the b-value anomaly at 100 km depth in the Alaska and New Zealand subduction zones. Geophys Res Lett 23:1557–1560

Wiemer S, McNutt S, Wyss M (1998) Temporal and three-dimensional spatial analysis of the frequency-magnitude distribution near Long Valley Caldera. J Geophys Int 134:409–421

Woodward-Clyde Consultants (1985) Earthquake activity and dam stability evaluations for the Aswan High Dam, Egypt, vol 3: seismic geology and tectonic studies of the Aswan Region, report to High Aswan Dam

Youssef MI (1968) Structural pattern of Egypt and its interpretation. AAPG Bull 52(4):601–614

Zedan TH, Osman HM, Osman MK (2002) Improving flood control capacity of high Aswan Dam and elevation of flooding. Dam maintenance and rehabilitation. Swets & Zeitlinger, Lisse, The Netherlands